Medical Engineering and Physics 000 (2016) 1–12

Contents lists available at ScienceDirect

Medical Engineering and Physics

journal homepage: www.elsevier.com/locate/medengphy

A patient-controlled functional electrical stimulation system for arm weight relief☆

C. Klauer[a,*], S. Ferrante[b], E. Ambrosini[b], U. Shiri[c], F. Dähne[c], I. Schmehl[c], A. Pedrocchi[b], T. Schauer[a]

[a] Control Systems Group, Technische Universität Berlin, Berlin, Germany
[b] NeuroEngineering and Medical Robotics Laboratory, NearLab, Politecnico di Milano, Milan, Italy
[c] Klinik für Neurologie mit Stroke Unit und Frührehabilitation, Unfallkrankenhaus, Berlin, Germany

ARTICLE INFO

Article history:
Received 8 January 2016
Revised 18 April 2016
Accepted 7 June 2016
Available online xxx

Keywords:
Signal processing
Medical systems
Biomedical control
Rehabilitation
Functional electrical stimulation
Electromyography

ABSTRACT

A patient-driven control strategy for Functional Electrical Stimulation (FES), which amplifies volitionally-initiated shoulder abductions, is proposed to improve stroke patients' rehabilitation. Based on the measured abduction angle, a FES-induced muscle recruitment is generated that yields a pre-specified percentage of this angle – yielding arm weight relief. To guarantee the correct recruitment also under fatigue and uncertain muscle activation we employ feedback control of the recruitment level determined by filtering the FES-evoked electromyogram. Filter parameters are user-optimized to obtain a linear relation between filter output and angle with a good signal-to-noise ratio. The auto-tuned recruitment controller (RC) was tested on five healthy subjects and compared to direct stimulation (DS) while muscle fatigue progressively occurred. Results showed a more linear relation between recruitment level and angle than between non-controlled stimulation intensity and angle ($R^2 = 0.93$ vs. $R^2 = 0.79$, angular range of 54°). After 6 min of stimulation, abduction decreased by 42% ± 14 for DS and by 0% ± 12 for RC, showing an effective compensation of fatigue. RC yielded significant smaller errors than DS in generating desired angles (0.23% ± 5.9 vs. 14.6% ± 9.7). When FES-induced arm weight support was provided, a mean reduction of the volitional effort (determined by Electromyography) of 78% was achieved compared to angular tracking without FES. First experiments with one acute stroke patient are also reported.

1. Introduction

Functional Electrical Stimulation (FES) is widely used for the rehabilitation or assistance of patients affected by neurological diseases [1]. It artificially activates paretic muscles during functional tasks by electrical stimulation of intact lower motor neurons. The increased afferent feedback provided by FES is known to modulate motor cortex function and excitability to enable recovery [2]. Recent studies [3,4] advocated the use of FES co-incidentally with the voluntary drive to enhance even more the plasticity of the central nervous system, so as to further improve its therapeutic effects [5].

One way to achieve synchronization between FES and volitional activity is to use myo-controlled neuroprostheses, in which the residual volitional EMG signal of the paretic muscle is used to control the timing and the intensity of the stimulation of the muscle itself [5]. Different strategies to control FES based on the residual EMG of the stimulated muscle were proposed in the literature. EMG-triggered controllers, which trigger the onset of a predetermined stimulation sequence applied in an open loop modality based on the volitional EMG, were firstly designed [6,7]. These systems are easy to implement and clinically feasible but do not actually assure the synchronization of FES and the intended voluntary movement after the trigger. This drawback is overcome by EMG-proportional controllers, which modulate the stimulation proportionally to the volitional EMG [8,9] and thus amplify weak residual muscle activity. However, this solution is less feasible on patients because it requires smooth muscle contractions to prevent oscillations caused by the closed-loop control system. An on/off non-linear control system was recently proposed [10]: it allows even patients with reduced muscle contractions to autonomously activate and deactivate the stimulation support exploiting their residual muscle activity, but it can lead to imprecise motor control.

☆ This work was partially funded by the German Federal Ministry of Education and Research (BMBF) within the project BeMobil (FKZ 16SV7069K) and by European project RETRAINER (Horizon 2020, Research and Innovation Programme, grant agreement no. 644721).

* Corresponding author. Tel.: +49 3031422276.
E-mail address: klauer@control.tu-berlin.de (C. Klauer).

http://dx.doi.org/10.1016/j.medengphy.2016.06.006
1350-4533/

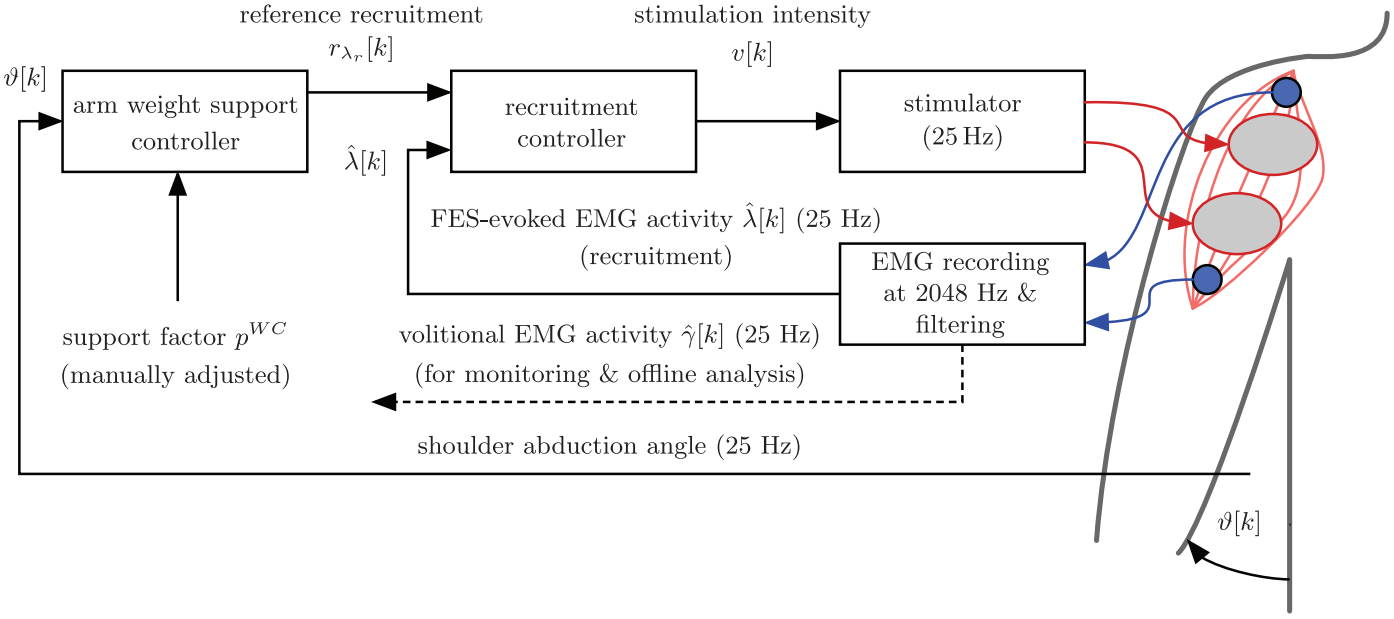

Fig. 1. Control scheme to achieve arm weight support by stimulation of the medial deltoid muscle.

A different approach to use FES co-incidentally with the voluntary drive, is to measure the desired target posture and to derive by means of an inverse mechanical model the joint moments required to achieve and to maintain that posture [11]. Then, partial or full support can be obtained by producing these moments partially or fully by means of FES. Compared to EMG-proportional stimulation, less precise muscular control is demanded from the patient. However, this approach requires precise neuro-musculoskeletal models to determine the desired stimulation intensities. Such models are difficult to obtain in clinical practice.

For repetitive tasks within a tightly controlled environment, Iterative Learning Control (ILC) can be applied to find the correct FES support in presence of residual muscle activity [12]. From trial to trial, ILC adjusts the stimulation intensity in order to improve the performance based on the measured joint angles from the previous trial.

The majority of FES-controlled systems use the stimulation intensity as control signal and solely observe the stimulation effect by measuring joint angles. Such control systems are slower than physiological movement control where forces and velocities are internally sensed by Golgi tendon organs and muscle spindles, respectively. In addition, when multichannel FES is delivered to obtain complex movements, the measure of the resulting angles is a global measure that is not able to sense the condition, e.g. muscle fatigue, of the stimulated muscles. Moreover, by solely using joint angles to measure the movement induced co-incidentally by FES and the patient it is not possible to distinguish between the volitional effort and the contribution provided by FES.

In a previous work [13], we proposed the use of FES-evoked EMG to assess the level of FES-induced muscle recruitment and to incorporate feedback control of it into FES systems. In our recent work [14], we could demonstrate in a case study on one healthy subject that such recruitment control enables the precise delivery of a desired movement support also in presence of muscular fatigue up to the maximal possible stimulation intensity that is adjusted by the controller. The desired support could be administrated synchronously to the voluntary muscle contractions in a repetitive tracking task and was modulated depending on the tracking performance and the observed volitional EMG activity. Additionally expected advantages of the recruitment control are the linearization of the of nonlinear muscle dynamics and the reduction of hysteresis effects in the muscle activation [13].

In this contribution, we propose a patient-driven control strategy, similar to that reported by Riener and Fuhr [11], which amplifies weak voluntary initiated shoulder abductions by providing an adjustable virtual arm weight support. Based on the measured abduction angle, a FES-induced muscle recruitment is generated that yields a pre-specified percentage of this angle. The use of recruitment control deliberates from obtaining complex muscle models as previously required [11]. A fast auto-tuning procedure for the EMG filter, applied on FES-evoked EMG, and for the recruitment controller is introduced. The performance of the employed underlying recruitment control is investigated in a study with healthy subjects with respect to the linearization of the system behavior and to the long-term generation of desired movement support also when muscle fatigue occurs. The maximal achievable arm weight support is determined by observing the reduction of volitional EMG activity during a user-controlled angle tracking task. In contrast to our previous work and ILC, the proposed approach is not restricted to repetitive tasks which renders its use more versatile. The feasibility of the proposed control strategy was finally demonstrated in a case study with one acute stroke patient.

2. Methods

2.1. System overview

The proposed control scheme, shown in Fig. 1, is intended to support patients with a weakness in shoulder abduction. FES is applied to the medial part of the deltoid muscle using a current-controlled stimulator (Rehastim, Hasomed GmbH, Germany) and self-adhesive electrodes (ValuTrode® CF4090 (4 × 9 cm), Axelgaard Manufacturing Co., USA). A stimulation frequency of 25 Hz was used and corresponded to the sampling frequency of the control system (sampling index k). The control signal $v[k] \in [0, 1]$ is

Please cite this article as: C. Klauer et al., A patient-controlled functional electrical stimulation system for arm weight relief, Medical Engineering and Physics (2016), http://dx.doi.org/10.1016/j.medengphy.2016.06.006

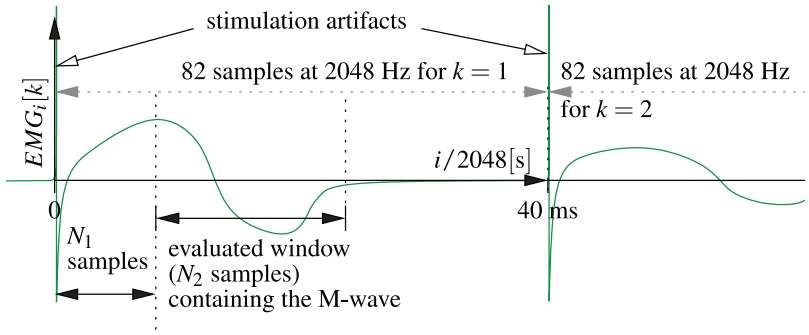

Fig. 2. Evaluation of the M-Wave to estimate the recruitment level.

the normalized pulse charge[1] q varying between zero and the maximally tolerable charge q_{max}. Increases in the pulse charge lead to equal increases in the pulse width and current amplitude [14]. The abduction angle $\vartheta[k]$ is measured at 25 Hz by means of an inertial sensor (MTx, Xsens Technologies B.V., The Netherlands). During active FES, the electromyogram (EMG) is measured at 2048 Hz (sampling index i) using separate Ag/AgCl electrodes (Ambu Neuroline 720, Ambu A/S, Denmark) and amplified using a multi-channel signal amplifier (Porti 32^{TM}, TMS International, The Netherlands). The EMG electrodes are placed outside the stimulation electrodes, as indicated in Fig. 1. By filtering the EMG (sampled at 2048 Hz), the volitional muscle activity level $\hat{\gamma}[k]$ and the muscle recruitment level $\hat{\lambda}[k]$ of the preceding stimulation period are obtained at stimulation frequency (cf. Sections 2.2.2 and 2.2.3). The recruitment controller adjusts the stimulation intensity to produce a desired recruitment level $r_{\hat{\lambda}}[k]$ that is generated by the angle-dependent arm weight support. The volitional EMG activity level is used to evaluate the performance of the arm weight support. The movement is patient-initiated by his/her weak residual muscle activity.

2.2. EMG signal processing

The FES-evoked and the volitional muscle activities are monitored by EMG of the deltoid muscle. The EMG is sampled at 2048 Hz yielding the raw EMG vector

$$\boldsymbol{EMG}_{raw}[k] = [EMG_{raw,1}[k] \cdots EMG_{raw,L}[k]]^T, L = 82,$$

for each stimulation sampling instant k. This vector captures an amount of $L = 82$ EMG samples of the preceding 40 ms inter-pulse interval (corresponding to 25 Hz stimulation frequency). As indicated in Fig. 2, the beginning is aligned to the stimulation pulse and contains information about the muscle activity related to the stimulus $k-1$. It is assumed that the FES-evoked EMG component (also called M-wave) is a time-variant signal in the mV-range while the volitional EMG signal part is band-limited Gaussian noise in the μV range. To separate both information, several signal processing steps need to be performed (adapted from [10] and [13]) as detailed in what follows.

2.2.1. Offset reduction

By calculating the offset in the raw EMG measurement by averaging the last three EMG samples of a stimulation period over the last five stimulation periods, this estimate is made robust against volitional EMG:

$$\hat{EMG}_{ofs}[k] = \frac{1}{5 \cdot 3} \sum_{j=k-5}^{k-1} \sum_{i=L-2}^{L} EMG_{raw,i}[j]. \quad (1)$$

No FES-evoked activity is expected in this time interval. Offset correction is performed by

$$\boldsymbol{EMG}[k] = \boldsymbol{EMG}_{raw}[k] - \hat{EMG}_{ofs}[k]. \quad (2)$$

2.2.2. Volitional EMG

The estimation of the volitional EMG during active FES requires the removal of the M-wave from the EMG signal. In the chosen approach, the EMG vectors of the last six stimulation periods are recorded. The best prediction of the currently measured EMG vector by a linear combination of the old stored EMG vectors is then used as estimate of the current M-wave. The corresponding weight parameters are optimized by a linear least squares approach at each stimulation period. Finally, the obtained estimate of the M-wave is subtracted from the currently measured EMG vector to determine the volitional EMG component, which is then evaluated by means of the 1-norm. This separation approach works better for the second half of the stimulation period where only the tail of the M-wave is contained. A detailed description of the procedure is given below.

Initially, the first 40 entries of the EMG measurement vector ***EMG[k]*** are set to zero to blank stimulation artifacts and to remove the main part of the M-wave during each inter-pulse interval. The last 10 samples are also not considered as their transmission from the EMG device to the PC via USB might not always be completed yielding

$$\boldsymbol{EMG}^{Vb}[k] = [\boldsymbol{0}_{40}^T \quad EMG_{41}[k] \quad \cdots \quad EMG_{L-11}[k]\boldsymbol{0}_{10}^T]^T \quad (3)$$

whereby $\boldsymbol{0}_{40}$ and $\boldsymbol{0}_{10}$ are zero vectors of the dimension 40 and 10, respectively.

Then, the vector $\boldsymbol{EMG}^{Ve}[k]$, containing the FES-evoked EMG response (M-wave), for the non-blanked sampling instants is estimated by applying the adaptive filter

$$\boldsymbol{EMG}^{Ve}[k] = [\boldsymbol{EMG}^{Vb}[k-1] \quad \cdots \quad \boldsymbol{EMG}^{Vb}[k-M]] \begin{bmatrix} \hat{p}_1^V[k] \\ \vdots \\ \hat{p}_M^V[k] \end{bmatrix} \quad (4)$$

where $\hat{\boldsymbol{p}}^V[k] = [\hat{p}_1^V[k] \quad \ldots \quad \hat{p}_M^V[k]]^T$ is continuously determined by solving the following least squares problem for each sampling instant k:

$$\hat{\boldsymbol{p}}^V[k] = \arg\min_{\boldsymbol{p}^V}[k]||\boldsymbol{EMG}^{Vb}[k] - [\boldsymbol{EMG}^{Vb}[k-1] \quad \cdots \quad \boldsymbol{EMG}^{Vb}[k-M]]\boldsymbol{p}^V||_2. \quad (5)$$

[1] The pulse charge q is defined of as product of the current amplitude I and pulse width pw of the first part for the symmetric bi-phasic pulse.

According to the investigations in [10], the number of previous EMG vectors is set to $M = 6$.

A scalar measure for the volitional muscle activity of the preceding 40 ms inter-pulse interval at sample k is obtained by taking the scaled 1-norm of the vector $(\boldsymbol{EMG}^{Vb}[k] - \boldsymbol{EMG}^{Ve}[k])$:

$$\hat{\gamma}[k] = 1/(L-50)\left|\left|\boldsymbol{EMG}^{Vb}[k] - \boldsymbol{EMG}^{Ve}[k]\right|\right|_1.$$

Hence, the volitional EMG part is the residual part of $\boldsymbol{EMG}^{Vb}[k]$ that can not be described by a linear combination of old blanked/filtered EMG vectors.

2.2.3. FES-evoked EMG

Similar to the approach described in Section 2.2.2, an estimate of the M-wave is obtained by using a linear combination of six previous EMG vectors. Then, the 1-norm is taken to obtain the intensity of the estimated M-wave in a sub-window of the inter-pulse interval. A detailed description of the procedure is given below.

To evaluate the M-wave, as shown in Fig. 2, the measured EMG is blanked yielding

$$\boldsymbol{EMG}^{Eb}[k] = [\boldsymbol{0}_{N_1}^T \;\; EMG_{N_1}[k] \;\; \cdots \;\; EMG_{N_1+N_2-1}[k] \;\; \boldsymbol{0}_{L-N_1-N_2}^T]^T, \quad (6)$$

whereby the parameters N_1 and N_2 describe window position and length, respectively. Analog to the voluntary filter, the evoked EMG component is predicted by an adaptive filter

$$\boldsymbol{EMG}^{Ee}[k] = [\boldsymbol{EMG}^{Eb}[k-1] \;\; \cdots \;\; \boldsymbol{EMG}^{Eb}[k-M]] \begin{bmatrix} \hat{p}_1^E[k] \\ \vdots \\ \hat{p}_M^E[k] \end{bmatrix} \quad (7)$$

where $\hat{\boldsymbol{p}}^E[k] = [\hat{p}_1^E[k] \;\ldots\; \hat{p}_M^E[k]]^T$ is continuously determined by solving the following least squares problem for each sampling instant k:

$$\hat{\boldsymbol{p}}^E[k] = \arg\min_{\boldsymbol{p}^E}[k]||\boldsymbol{EMG}^{Eb}[k] - [\boldsymbol{EMG}^{Eb}[k-1] \;\; \cdots \;\; \boldsymbol{EMG}^{Eb}[k-M]]\boldsymbol{p}^E||_2. \quad (8)$$

Then, the one-norm of $\boldsymbol{EMG}^{Ee}[k]$ yields the estimated muscular recruitment level

$$\hat{\lambda}_{N_1,N_2}[k] = \left|\left|\boldsymbol{EMG}^{Ee}[k]\right|\right|_1.$$

Both parameters are adapted to the individual user by the optimization procedure outlined in Section 2.4.

2.3. Recruitment control

To design the controller, the following simplified, linear discrete-time model, describing the relation between the stimulation intensity v and the estimated recruitment $\hat{\lambda}$, is assumed:

$$\hat{\lambda}(k) = \Theta_{r,a}\, q^{-1}\, v(k) + \Theta_{r,b} + e(k), \quad \Theta_{r,a} > 0,\; 0 \le v(k) \le 1. \quad (9)$$

Here, q^{-1} is the backward-shift operator $(a(k)q^{-1} = a(k-1))$ and $e(k)$ is white noise (variance $\sigma_{\hat{\lambda}}^2$, expected value is zero). This equation describes the linear, rising part of the non-linear recruitment function show in Fig. 3. The time delay of one sampling instant is introduced because the estimate $\hat{\lambda}[k+1]$ depends on the stimulation pulse $v[k]$ applied for the previous sampling instant k.

The parameters $\Theta_{r,a}$ and $\Theta_{r,b}$ are adapted by Least Squares to match recorded data pairs describing the linear part of the recruitment function. This dataset is obtained in a calibration procedure outlined in Section 2.4.

Frequency Domain Controller Synthesis. During control, the offset $\Theta_{r,b}$ of the linear model (9) is treated as a part of the constant disturbance.

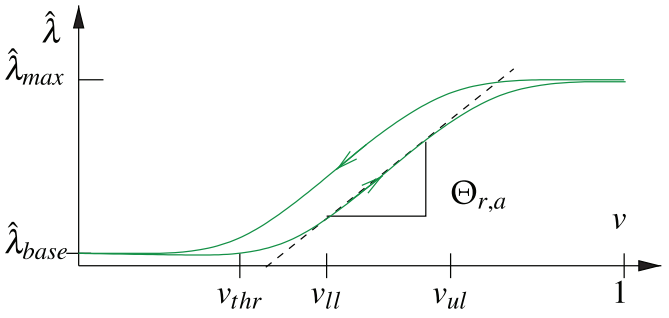

Fig. 3. Muscular recruitment function including hysteresis and the used linear approximation for the stimulation range $[v_{ll}, v_{ul}]$. Further, $\hat{\lambda}_{base}$ is the base level that occurs when stimulation not leading to a muscle contraction is applied. The maximally obtained value for $\hat{\lambda}$ is called $\hat{\lambda}_{max}$ and v_{thr} is the stimulation intensity yielding the onset of muscle contraction.

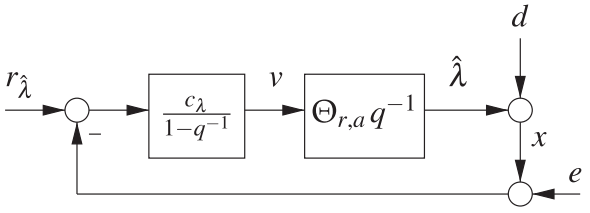

Fig. 4. Recruitment controller applied to the nominal plant.

To control the nominal plant $G(q^{-1}) = \Theta_{r,a}\, q^{-1}$, a discrete-time integrating controller is chosen:

$$K(q^{-1}) = \frac{c_\lambda}{1-q^{-1}}, \quad c_\lambda > 0.$$

The resulting closed-loop behavior (cf. Fig. 4.) between the reference and the output $\hat{\lambda}$ is described by

$$T(q^{-1}) = \frac{GK}{1+GK} = \frac{\Theta_{r,a}c_\lambda\, q^{-1}}{1+(\Theta_{r,a}c_\lambda - 1)\, q^{-1}}.$$

The control system is stable if the root $q_\infty = 1 - \Theta_{r,a}c_\lambda$ of the closed loop polynomial $1 + (\Theta_{r,a}c_\lambda - 1)\, q^{-1}$ fulfills $0 < q_\infty < 1$, which is equivalent to $0 < \Theta_{r,a}c_\lambda < 1$.

To be able to adjust the noise transmission of the closed loop, we introduce the tunable parameter T_n describing the noise amplification at the Nyquist-frequency. It is calculated using the complementary sensitivity transfer function T (defined as the transfer function between $-e$ and x) that is evaluated at the Nyquist-frequency $(q = -1)$:

$$T_n = |T(q^{-1} = -1)| = \frac{|-\Theta_{r,a}c_\lambda|}{|2 - \Theta_{r,a}c_\lambda|} = \frac{\Theta_{r,a}c_\lambda}{2 - \Theta_{r,a}c_\lambda}, \quad \text{for } 0 < q_\infty < 1. \quad (10)$$

This equation is solved w.r.t to c_λ.

$$c_\lambda = \frac{1}{\Theta_{r,a}} \frac{2T_n}{T_n + 1}. \quad (11)$$

To obtain an asymptotically stable closed loop $(0 < q_\infty < 1 \Leftrightarrow 0 < \Theta_{r,a}c_\lambda < 1)$, the tunable parameter T_n must fulfill

$$0 < T_n < 1. \quad (12)$$

The tuning parameter T_n is chosen such that the amplification of high frequent measurement noise at the Nyquist-frequency with an amplitude $\sigma_{\hat{\lambda}}$ (standard deviation of the noise e estimated for the model (9) by T_n results in 1% of the maximal signal amplitude λ_{max}:

$$0.01\lambda_{max} = T_n\sigma_{\hat{\lambda}}. \quad (13)$$

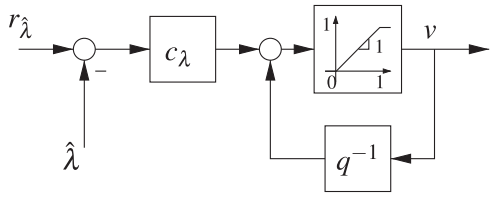

Fig. 5. Recruitment controller with anti-windup strategy.

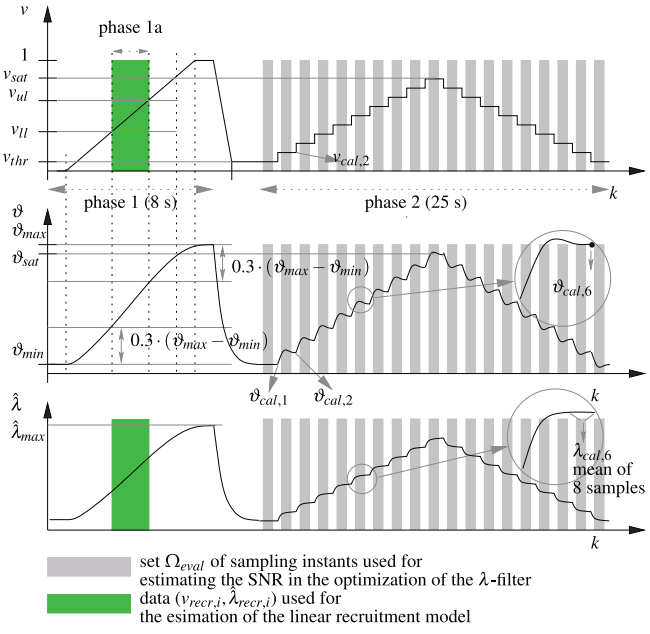

Fig. 6. Calibration Experiment: During phase 1, a linear increasing stimulation intensity is applied up to the maximal tolerable intensity and in phase 2, a stair-wise increase and decrease of the stimulation intensity is performed. The characteristic stimulation intensities v_{thr} and v_{sat} obtained in phase 1 are used to parameterize the stimulation ranges in phase 2. The EMG- and joint angle data obtained during phase 2 are used to optimize the λ-filter and afterwards $\hat{\lambda}$, the output of the optimal filter, is calculated. Finally the dataset $(v_{recr,i}, \hat{\lambda}_{recr,i})$ used for the identification of the linear recruitment model and the dataset $(\hat{\lambda}_{cal,s}, v_{cal,s}, \vartheta_{cal,s})$, describing the static actuation to joint angle relationships are extracted.

By resorting Eq. (13) and inserting into Eq. (11) we obtain:

$$c_\lambda = \frac{1}{\Theta_{r,a}} \frac{2\lambda_{max}}{\lambda_{max} + 100\sigma_{\hat{\lambda}}}. \tag{14}$$

This selection gives the fastest possible closed-loop behavior for the specified SNR at the Nyquist-frequency.

Anti-Windup. Since the actuation variable is bounded by $v \in [0, 1]$ and because of the integrating controller, an anti-windup strategy as shown in Fig. 5 is used to avoid undesired closed-loop behavior in case of saturation [15].

2.4. Autotuning of recruitment (λ) control

2.4.1. Procedure

An automatic calibration procedure is carried out prior to each session in order to obtain the linear model of the recruitment function and to tune the filter parameters N_1, N_2 as well as the controller parameter c_λ.

The calibration procedure consists of two phases shown in Fig. 6, wherein the subject is asked not to intervene in the movement. During phase 1, the stimulation intensity is linearly increased from zero up to the maximum tolerated value and the EMG data, $\boldsymbol{EMG}_{p1}$, as well as the corresponding angle values, ϑ_{p1}, are recorded. From these data, the following values are calculated:

- ϑ_{min} – the minimal angle when no FES is applied.
- v_{thr} – the stimulation intensity leading to the onset of the FES-induced muscle contraction. v_{thr} is defined as the stimulation intensity corresponding to a $\hat{\lambda}$ value higher than its baseline, calculated when no FES is applied. Since the optimal parameters N_1 and N_2 have not been estimated at this point of the procedure, two generally valid values ($N_1 = 8$ and $N_2 = 20$) are used to estimate $\hat{\lambda}$.
- ϑ_{sat} – the stimulation intensity above which no significant joint angle increase occurs. v_{sat} is defined as the stimulation intensity leading to an angle equal to the 95% of the maximum angle achieved, ϑ_{max}.

During phase 2, the stimulation intensity is increased from v_{thr} to v_{sat} following a stair-wise signal consisting of 10 intermediate steps and the $\boldsymbol{EMG}_{p2}$ and ϑ_{p2} data are collected. These data are used to optimize the parameters N_1 and N_2, as described in Section 2.4.2. When the optimal parameters $\hat{N}_1$ and $\hat{N}_2$ are found, $\hat{\lambda}$ is calculated for both phases 1,2. The data $\hat{\lambda}$ and v obtained during phase 1 are then used to identify the linear recruitment model. To assure that these data belong to the linear range of the recruitment function, two additional values of stimulation intensities are defined:

- v_{ll} (lower bound), corresponding to an angle equal to $\vartheta_{min} + 0.3 \cdot (\vartheta_{max} - \vartheta_{min})$.
- v_{ul} (upper bound), corresponding to an angle equal to $\vartheta_{max} - 0.3 \cdot (\vartheta_{max} - \vartheta_{min})$.

The subset containing N_{recr} samples of data within the range $v \in [v_{ll}, v_{ul}]$ yields the dataset $(v_{recr,i}, \hat{\lambda}_{recr,i}, i = 1, 2, ..., N_{recr})$ that is used to identify the parameters $\Theta_{r,a}$ and $\Theta_{r,b}$ of the linear recruitment model (c.f. Fig. 3) described in Section 2.3.

Further, data sets describing the steady state stimulation intensity – angle and recruitment level – angle relationships are obtained from each stair during phase 2 as illustrated in Fig. 6 yielding $(\hat{\lambda}_{cal,s}, v_{cal,s}, \vartheta_{cal,s})$. Herein, $s = 1, 2, ..., 10$ corresponds to increasing- and $s = 11, 12, ..., 19$ to the decreasing stairs. The obtained data sets are later used in the arm weight compensation controller to obtain a static gain of a model describing the arm abduction (c.f. 2.5).

2.4.2. FES-evoked EMG filter optimization

The aim of this phase is to identify N_1 and N_2 assuring a high SNR of the estimated recruitment $\hat{\lambda}$ and a good linearity between $\hat{\lambda}$ and the purely FES induced torque. Under the assumption of small angles we can interpret the abduction angle as an indirect measure of the joint torque when the bio-mechanical system is in steady-state.

In an optimization procedure, the estimated recruitment signal $\hat{\lambda}_{p_2,N_1,N_2}$ is calculated from the EMG dataset $\boldsymbol{EMG}_{p_2}$ recorded during phase 2 for each possible combination of $N_1 \in [2, 20]$ and $N_2 \in [1, 30]$, which captures the feasible values for window positions and lengths. Then, for each signal $\hat{\lambda}_{p_2,N_1,N_2}$ the SNR and a measure of linearity w.r.t ϑ_{p2} is calculated as described in this section and finally the best parameters are selected.

Linearity between $\hat{\lambda}$ and ϑ. For the stationary relationship between $\hat{\lambda}$ and ϑ we assume a linear model of the form

$$\vartheta = \Theta_{\vartheta\lambda,N_1,N_2,a} \cdot \hat{\lambda}_{N_1,N_2} + \Theta_{\vartheta\lambda,N_1,N_2,b} + e_\vartheta \tag{15}$$

From the I/O dataset $(\hat{\lambda}_{p_2,N_1,N_2}, \vartheta_{p_2})$ one data pair is extracted for each stair s during the stationary phases of the bio-mechanical system. Therefore, at the end of the constant phase of each stair

s, the joint angle $\vartheta_{cal,\,s}$ is obtained and further the mean value of $\hat{\lambda}_{p_2,N_1,N_2}$ over 8 samples at the end of the constant phase is calculated yielding $\hat{\lambda}_{cal,s,N_1,N_2}$ as illustrated in Fig. 6. Using this dataset, the model parameters $\Theta_{\vartheta\lambda,N_1,N_2,a}$ and $\Theta_{\vartheta\lambda,N_1,N_2,b}$ are identified by least squares. Then, the obtained model is used to compute the joint angles $\hat{\vartheta}_{s,N_1,N_2}$ for each stair s, which is then compared to the measured angles $\vartheta_{cal,\,s}$ by calculating the Normalized Root Mean Square Error (NRMSE) that serves as a measure of linearity:

$$NRMSE_{N_1,N_2} = \frac{\sqrt{\frac{1}{N_s}\sum_{s=1}^{N_s}(\vartheta_{cal,s} - \hat{\vartheta}_{s,N_1,N_2})^2}}{\max_s \vartheta_{cal,s} - \min_s \vartheta_{cal,s}}, \tag{16}$$

whereby $N_s = 19$ denotes the number of stairs cases.

Estimation of the Signal to Noise Ratio (SNR). Since the noise-free signal for $\hat{\lambda}_{p_2,N_1,N_2}$ is not available, the signal component is estimated by applying a non-causal 2nd order Butterworth low-pass filter with zero phase shift, $f_{cut} = 75$Hz to $\hat{\lambda}_{p_2,N_1,N_2}$ yielding $\lambda_{lp,p_2,N_1,N_2}[k]$.

The estimated noise signal $\hat{e}_{\hat{\lambda}}$ is then calculated by

$$\hat{e}_{\hat{\lambda},N_1,N_2} = \hat{\lambda}_{p_2,N_1,N_2} - \lambda_{lp,p_2,N_1,N_2}. \tag{17}$$

The power of the signal and the noise component are then evaluated based on the time-series λ_{lp,p_2,N_1,N_2} and $\hat{e}_{\hat{\lambda},N_1,N_2}$ respectively.

Because the filter introduces transients starting from both borders of the dataset (due to uninitialized initial values of the non-causal filter), 20 samples are skipped for the computation of the signal power at each border respectively. Further, due to the steps in the excitation signal v, frequency components even beyond the cutting frequency f_{cut} are present in $\hat{\lambda}_{p_2,N_1,N_2}$ actually belonging to the signal component. No clean separation is possible with a low pass filter for these frequency components. Hence, the sampling instants of the time-series signal close to the stepwise changes (6 samples before and after the step) are additionally not considered for the calculation of signal and noise power. Finally, the calculation is only performed in the set Ω_{eval} including $N_{\Omega_{eval}}$ samples (c.f. Fig. 6). The signal power is calculated by

$$P_{s,N_1,N_2} = \frac{1}{N_{\Omega_{eval}}} \sum_{i\in\Omega_{eval}} |\lambda_{lp,N_1,N_2}[i]|^2. \tag{18}$$

Similar, the noise power is then given by

$$P_{n,N_1,N_2} = \frac{1}{N_{\Omega_{eval}}} \sum_{i\in\Omega_{eval}} |\hat{e}_{\hat{\lambda},N_1,N_2}[i]|^2. \tag{19}$$

Finally, the SNR is then calculated for each filter variation by

$$SNR_{N_1,N_2} = \frac{P_{s,N_1,N_2}}{P_{n,N_1,N_2}}. \tag{20}$$

Quality functions. Both measures SNR_{N_1,N_2} and $NRMSE_{N_1,N_2}$ are combined in a quality function in form of a weighted sum using a tunable factor p_w to adjust the importance of the individual measures:

$$J_{N_1,N_2} := p_w \cdot \underbrace{(1 - NRMSE_{N_1,N_2})}_{J_1} + (1 - p_w) \cdot \underbrace{\frac{SNR_{N_1,N_2}}{\max_{N_1,N_2}(SNR_{N_1,N_2})}}_{J_2}. \tag{21}$$

Herein, the SNR is normalized w.r.t to the observed maximum. Thus, for both sub functions J_1 and J_2, the optimal values describing the best SNR respectively and the best linearity are represented by $J_1 = 1$ and $J_2 = 1$, respectively. Hence, the comparison in the weighted sum is possible. A weighting factor of $p_w = 0.9$ is chosen, because a linear relationship is considered to be more important

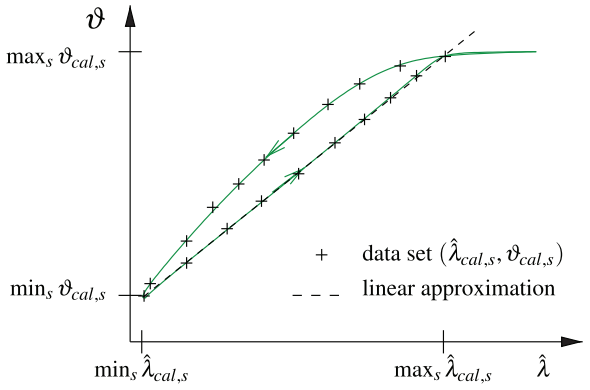

Fig. 7. Relation between $\hat{\lambda}$ and ϑ for the data set $(\hat{\lambda}_{cal,s},\ \vartheta_{cal,\,s})$ obtained during the calibration procedure of the recruitment controller.

for the arm weight support controller. To find the optimal compromise, the maximum of J_{N_1,N_2} is obtained by variating the tunable filter parameters N_1 and N_2 yielding the optimal parameters

$$[\hat{N}_1, \hat{N}_2]^T = \arg\max_{N_1,N_2} J_{N_1,N_2}, \text{ whereby } \hat{J} = J_{\hat{N}_1,\hat{N}_2}. \tag{22}$$

Ongoing, we shorten the notation of the optimal estimate to $\hat{\lambda} := \hat{\lambda}_{\hat{N}_1,\hat{N}_2}$.

2.4.3. Recruitment controller parameterization

The estimated parameters $\Theta_{r,\,a}$ and $\Theta_{r,\,b}$ of the linear recruitment model and the standard deviation $\sigma_{\hat{\lambda}}$ of the noise are used to determine c_{λ} by Eq. (14). Therefore, $\sigma_{\hat{\lambda}}$ is estimated from the estimated noise $\hat{e}_{\hat{\lambda},\hat{N}_1,\hat{N}_2}$ by

$$\sigma_{\hat{\lambda}} = \sqrt{\frac{1}{N_{\Omega_{noise}}} \sum_{k\in\Omega_{noise}} (\mu_e - \hat{e}_{\hat{\lambda},\hat{N}_1,\hat{N}_2}[k])^2},$$
$$\mu_e = \frac{1}{N_{\Omega_{noise}}} \sum_{k\in\Omega_{noise}} \hat{e}_{\hat{\lambda},\hat{N}_1,\hat{N}_2}[k]. \tag{23}$$

2.5. FES arm weight support

The aim of the proposed control system is to induce a fraction p^{WC} of the currently measured arm abduction by FES. In turn, this leads to a reduced voluntary effort.

The typical relationship for the $\hat{\lambda}$ – angle relation described by the data set $(\hat{\lambda}_{cal,s},\ \vartheta_{cal,\,s})$ is shown in Fig. 7. As known from previous experimental experience, typically, hysteresis effects may be present in this relation. In the design of the weight compensating control system, at first, we approximately assume a linear relationship for the steady state $\hat{\lambda}$ – angle relation:

$$\vartheta = (\hat{\lambda} - \min_s \hat{\lambda}_{cal,s}) \frac{\max_s \vartheta_{cal,s} - \min_s \vartheta_{cal,s}}{\max_s \hat{\lambda}_{cal,s} - \min_s \hat{\lambda}_{cal,s}} + \min_s \vartheta_{cal,s}.$$

Let us introduce the abbreviations

$$\lambda^{WC}_{min} := \min_s \hat{\lambda}_{cal,s} \quad \lambda^{WC}_{max} := \max_s \hat{\lambda}_{cal,s} \tag{24}$$

$$\vartheta^{WC}_{min} := \min_s \vartheta_{cal,s} \quad \vartheta^{WC}_{max} := \max_s \vartheta_{cal,s}. \tag{25}$$

To support arm weight, a linear mapping of joint angles within a range $\Omega_{\vartheta} := [\vartheta^{WC}_{min}, \vartheta^{WC}_{max}]$ to the virtual actuation variable[2] $r_{\hat{\lambda}} \in \Omega_{\hat{\lambda}}$ in the range $\Omega_{\hat{\lambda}} := [p^{WC}\lambda^{WC}_{min}, p^{WC}\lambda^{WC}_{max}]$ is performed. The controller gain $p^{WC} \in [0, 1]$ is called support factor. Additionally, $r_{\hat{\lambda}}$ is

[2] The reference of the underlying recruitment controller.

Please cite this article as: C. Klauer et al., A patient-controlled functional electrical stimulation system for arm weight relief, Medical Engineering and Physics (2016), http://dx.doi.org/10.1016/j.medengphy.2016.06.006

saturated in case it exceeds the limits of ϑ^{WC}_{min} and ϑ^{WC}_{max}. The controller is then given by

$$r_\lambda = \mathrm{sat}_{\lambda^{WC}_{min},\lambda^{WC}_{max}}\left(\frac{p^{WC}\lambda^{WC}_{max} - p^{WC}\lambda^{WC}_{min}}{\vartheta^{WC}_{max} - \vartheta^{WC}_{min}}(\vartheta - \vartheta^{WC}_{min}) + p^{WC}\lambda^{WC}_{min}\right). \tag{26}$$

Under the assumption of 2nd-order linear time-invariant plant dynamics without transmission zeros, the closed-loop system is asymptotically stable for $0 \le p^{WC} < 1$. As p^{WC} tends to one, the required voluntary activity theoretically tends to zero.

The support factor p^{WC} is manually adjusted during the experiment to obtain the desired behavior. Because of the present hysteresis and remaining nonlinearity in the static recruitment – angle relationship, the practically achievable maximal support p^{WC} not causing overcompensation is limited to a value slightly below 1 (theoretical full support). One aim of this study is to determine the limits in healthy subjects.

2.6. Validation procedures

2.6.1. Validation of the auto-tuned RC

The performance of the auto-tuned RC was compared to direct stimulation (DS). To perform this comparison, a long term test was designed in which single trials using alternatively the auto-tuned RC and the DS were repeated until significant muscle fatigue occurred. Tests were carried out on healthy subjects who were asked not to intervene voluntarily in the movement. During each trial j, a pre-defined sequence of 19 reference joint angles with $s = 1, 2, \ldots, 19$ were used as reference input for the two controllers. For the first 10 references we chose a linearly increasing ramp between ϑ_{min} and $0.95 \cdot \vartheta_{max}$, while the last 9 references were chosen to decrease to ϑ_{min} with the same spacing. Using the calibration dataset ($\hat{\lambda}_{cal,s}$, $v_{cal,s}$, $\vartheta_{cal,s}$) the stimulation intensities v_s and the reference recruitment levels $r_{\hat{\lambda},s}$ that theoretically lead to the joint angles $\vartheta_{comp,s}$ were calculated. Successively, each of these values was constantly applied for 1s using DS and RC respectively. For each trial j, each stair s and each control type ($type \in \{DS, RC\}$), the resulting steady-state joint angles $\vartheta_{j,s,DS}$ and $\vartheta_{j,s,RC}$ caused v_s and $r_{\hat{\lambda},s}$, respectively, were measured directly before the next stepwise change in the actuation variable.

The following parameters were computed to compare DS and RC controllers:

a) Linearity. The degree of linearity was computed both during the RC calibration phase and during the fatigue test. During calibration, the steady-state dataset ($\hat{\lambda}_{cal,s}$, $v_{cal,s}$, $\vartheta_{cal,s}$) was analyzed comparing the degree of linearity obtained between the non-controlled direct stimulation intensity $v_{cal,s}$ and the angle $\vartheta_{cal,s}$ and between the recruitment level $\hat{\lambda}_{cal,s}$ and the angle $\vartheta_{cal,s}$. For each subject, linear models were identified for both relations and compared in terms of the fitting coefficient of determination, denoted R^2, and the normalized root mean squared error (NRMSE) between the fitted line and the dataset values. During the successive trials of the fatigue test, given that the 5 subjects performed a different number of trials before fatigue occurred, a mean degree of linearity was computed for each subject and was assessed by the coefficient of determination R^2. Only steps in which the stimulation intensity was not saturated were considered for the recruitment controller. To maximize comparability across subjects, before applying the linear fitting, the measured angles $\vartheta_{j,s,type}$ were normalized to their overall minimum $\underline{\vartheta}$ and maximum $\overline{\vartheta}$ value obtained by each subject:

$$\vartheta_{norm,j,s,type} = (\vartheta_{j,s,type} - \underline{\vartheta})/(\overline{\vartheta} - \underline{\vartheta}). \tag{27}$$

b) Fatigue. To evaluate the effect of muscle fatigue, we calculate the mean value of all normalized joint angles for the rising part of the stair-case:

$$M_{j,type} = 1/10 \cdot \sum_{s=1}^{s=10} \vartheta_{norm,j,s,type}, \quad \text{for } type \in \{DS, RC\}. \tag{28}$$

For both actuation types, we model the decaying of $M_{j,type}$ w.r.t the trial number j using the model

$$\hat{M}_{j,type} = F_{a,type}\, j + F_{b,type}. \tag{29}$$

The estimated drop of the mean angle after 8 trials is given by $DROP_{8,type} = 1 - \hat{M}_{8,type}/\hat{M}_{1,type}$, $type \in \{RC, DS\}$.

c) Hysteresis. For each trial j and for both controller types, we calculated the difference between the normalized joint angles obtained during the increasing stair-case except the last ($s = 1, 2, \ldots, 9$) and the respective angles caused by the same actuation level during decreasing stair-case. The absolute values of these differences were summed up and used to describe the intensity of the hysteresis as follows:

$$H_{j,type} = \sum_{i=1}^{i=9} |\vartheta_{norm,j,i,type} - \vartheta_{norm,j,10+9-i,type}| \tag{30}$$

d) Angle error. For each stair s and each trial j the error between the measured normalized angles and the desired value was calculated by

$$\vartheta_{norm,e,j,s,type} = \vartheta_{norm,r,comp,s} - \vartheta_{norm,j,s,comp,type}. \tag{31}$$

The mean value and standard deviation of $\vartheta_{norm,e,j,s,type}$ over all trials j and stairs s was then determined to describe the ability of the DS and RC controllers in generating the desired angles for longer time periods.

To compare the performance of the two controllers (DS and RC) separate Wilcoxon signed-rank tests were performed on the linearity evaluated in terms of R^2, the fatigue measured in terms of angle drop after 8 trials, the mean angle error and the hysteresis indexes.

2.6.2. Validation of the arm weight compensation

To find out the maximal possible support factor p^{WC} and to analyze the reduction of the voluntary activity required to perform a defined joint-angle tracking task in the angular range 0–60° under different levels of support, a trial-based test was carried out. While the weight compensation controller is activated, the subject is instructed to follow a stair-case like angular reference trajectory (three increasing and decreasing stairs respectively) visualized on a LCD-screen along with the currently measured joint angle during each trial. When healthy volunteers were involved in these tests, they were asked to provide the minimal effort needed to track the angular reference trajectory.

As the trial number increases, the support factor p^{WC} is increased by 10% per trial starting from zero support:

$$p^{WC}_j = (j-1) \cdot 0.1, \quad j = 1, 2, \ldots, N_t, \quad N_t \le 11.$$

The experiment is aborted when an overcompensation of the arm weight is observed, meaning the subject has to actively push down to decrease the abduction level.

For all trials, the voluntary EMG $\hat{\gamma}$ is calculated as described in Section 2.2.2 and applied to a low-pass filter (non-causal Butterworth filter of 2nd-order, with zero phase shift and a cutting frequency of 0.5 Hz) yielding $\hat{\gamma}_{lp}$. This signal is normalized to its respective minimum and maximum value yielding $\hat{\gamma}_{lp,norm}$. Finally, for each trial the corresponding sub-set is extracted yielding the signal $\hat{\gamma}_{lp,norm,j}$ for each trial j. Similar, ϑ_j is the signal for the measured joint angle during each trial j.

Please cite this article as: C. Klauer et al., A patient-controlled functional electrical stimulation system for arm weight relief, Medical Engineering and Physics (2016), http://dx.doi.org/10.1016/j.medengphy.2016.06.006

Table 1
Results of the filter optimization for neurologically intact subjects (S1 to S5) and the stroke patient P. The linearity of the actuation variable – angle relation is captured by the *NRMSE* and R^2 values for v and $\hat{\lambda}$ as input arguments, respectively.

Subject	N_1	N_2	*NRMSE* $v \to \vartheta$	*NRMSE* $\hat{\lambda} \to \vartheta$	R^2 $v \to \vartheta$	R^2 $\hat{\lambda} \to \vartheta$	*SNR*	Angular range [°]	Max. intensity: current [mA], pulsewidth [μs]
S1	8	23	0.145	0.082	0.853	0.953	2798	40.23	54, 270
S2	6	8	0.128	0.082	0.89	0.954	5329	35.99	38, 186
S3	7	13	0.131	0.072	0.892	0.967	6966	73.73	38, 181
S4	3	17	0.139	0.077	0.848	0.953	10450	46.76	52, 272
S5	5	13	0.114	0.075	0.893	0.954	7472	77.94	56, 282
P	6	18	0.116	0.071	0.914	0.968	14014	23.69	62, 326
Mean	5.8	15.3	0.129	0.076	0.87	0.96	7838	49.7	50, 253
Std	1.72	5.16	0.012	0.007			3938	21.6	10, 57

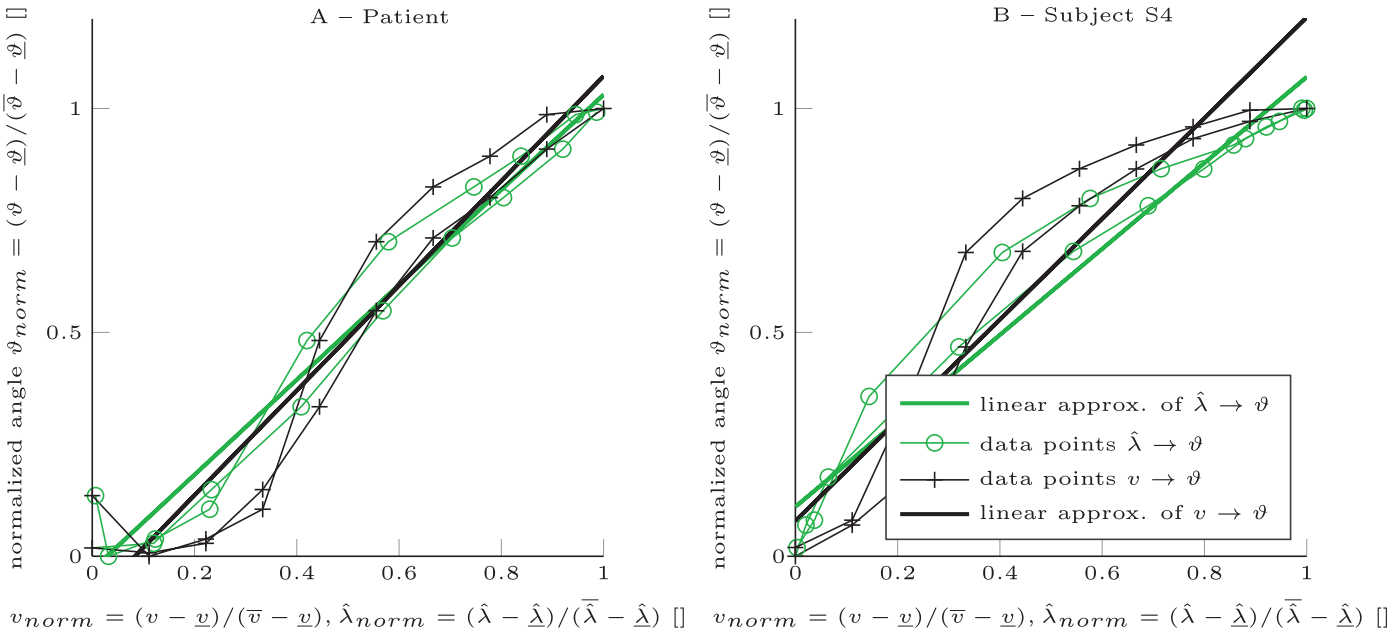

Fig. 8. Comparison of the achievable degree of linearity for the stroke patient (left) and the subject S4 (right). The linear regressions for the $v_{cal,s} - \vartheta_{cal,s}$ and the $\hat{\lambda}_{cal,s} - \vartheta_{cal,s}$ relationship are shown. In case of the $\hat{\lambda}$ – angle relationship, the normalized RMS-error has been significantly improved. All signals in the plot are normalized with respect to the observed minima and maxima of the analyzed data set.

To assess the required voluntary activity with respect to the actually achieved arm abduction, the quotient A_j of the mean value $\hat{\gamma}_{mean,j}$ of the voluntary EMG $\hat{\gamma}_{lp,norm,j}$ and the mean value $\vartheta_{mean,j}$ of the measured joint angle ϑ_j is calculated for each trial:

$$A_j := \hat{\gamma}_{mean,j}/\vartheta_{mean,j}, \quad j = 1, 2, ..., N_t,$$

which we call activity level. To allow a comparison across subjects, we perform a normalization to the maximal activity level:

$$A_{norm,j} = A_j / \max_j A_j.$$

For each subject we determine the maximal possible support level and minimal required activity level for fulfilling the tracking task.

3. Results and discussion

Five healthy male subjects (S1 to S5, age 32.8 ± 5.7 years) and one acute stroke patient (81 year old male, 6 days after infarct, with nearly complete arm abduction paralysis and completely lost hand functions) participated in the study. The trials have been approved by the ethics committee of the Berlin Chamber of Physicians (Ärztekammer Berlin). The test to analyze the influences of muscle fatigue and the weight compensation test were performed on different days for the healthy subjects, whereby the calibration procedures were performed directly before each test, respectively.

3.1. Recruitment control results

The results of the calibration procedure, directly performed before the fatigue test, are summarized in Table 1. Detailed results for the determined stimulation intensity – angle as well as $\hat{\lambda}$ – angle relationship are shown in Fig. 8 for the stroke patient and for one healthy subject, as representative. Across subjects, the optimization procedure yielded widely spread parameters N_1 and N_2 indicating the need for adaption to each individual. In all cases, the degree of linearity in terms of the NRMSE has been significantly improved (in average by 41%) when considering the $\hat{\lambda}$ – angle relation.

Results of the fatigue test (long-term comparison of DS and RC) are summarized in Table 2 for all healthy subjects. Reported are the hysteresis over all trials, the drop of the mean abduction angle over eight trials (6 min of active FES)[3], the measure of linearity

[3] Calculated based on a linear model approximation of the trial $j - M_j$, *type* relation.

Table 2
Comparison of non-controlled direct stimulation (DC) and recruitment control (RC). Analyzed are the static stimulation intensity – angle and recruitment level – angle relations which are obtained by ramping up and down repeatedly the stimulation intensity and the desired requirement level, respectively.

	Non-controlled direct stimulation (DS)				Recruitment control (RC)			
Subject	Hysteresis (mean ± std)	Linearity (R^2)	$DROP_8$ [%]	Angle error [%] (mean ± std)	Hysteresis (mean ± std)	Linearity R^2	$DROP_8$ [%]	Angle error [%] (mean ± std)
S1	18.08 ± 6.19	0.74	27.8	13.1 ± 7.0	14.29 ± 2.53	0.90	−4.9	−6.06 ± 11.33
S2	8.38 ± 5.82	0.78	55.1	9.8 ± 12.6	6.83 ± 5.80	0.92	11.8	−2.71 ± 3.84
S3	8.85 ± 5.81	0.74	57.0	13.2 ± 14.2	7.04 ± 2.45	0.93	−17.6	1.08 ± 5.56
S4	7.29 ± 0.94	0.78	41.7	25 ± 8.8	4.88 ± 1.85	0.97	9.1	9.2 ± 5.12
S5	3.37 ± 0.74	0.90	29.0	11.8 ± 6.0	4.56 ± 1.02	0.94	−0.5	−0.04 ± 3.84
Mean	9.2	0.79	42.11	14.6	7.52	0.93	−0.42	0.23
Std	5.41		13.83	9.7	3.94		11.7	5.8

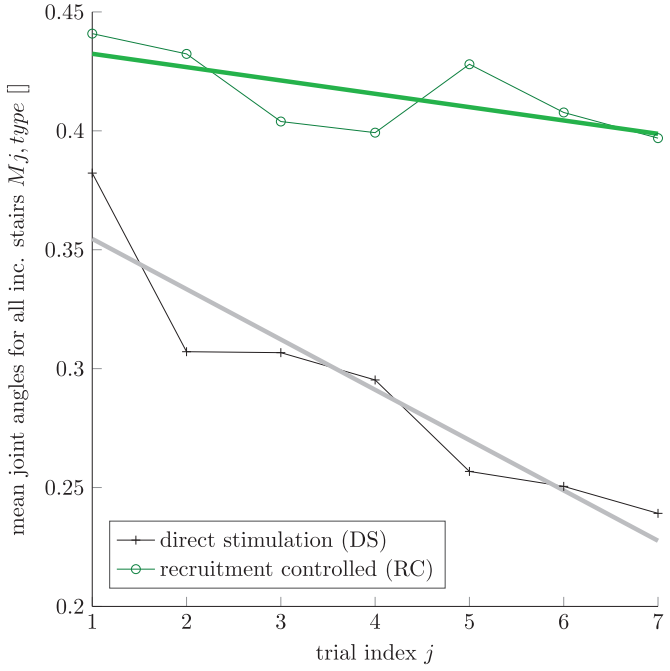

Fig. 9. Exemplary results of the fatigue comparison test for subject S4. For both control types and each trial j, the fatigue indicators $M_{j,\,DS}$ and $M_{j,\,RC}$ (normalized mean stationary angles of the rising part of the staircases) have been calculated respectively. As the number of trials increase, a significant decrease of the joint angle is observed, when using uncontrolled stimulation (DS). In case of λ-control however, the effect of muscle fatigue is compensated.

(R^2) for the actuation variable – angle relation, and the mean error between the desired angles and actual achieved angles.

A Wilcoxon signed-rank test showed that the use of recruitment control significantly improved linearity (R^2, $Z = -2.023$, $p = 0.043$), fatigue test ($DROP_8$, $Z = -2.023$, $p = 0.043$), and reduced the mean angle error ($Z = -2.023$, $p = 0.043$) with respect to the non-controlled direct stimulation.

The decrease of the mean abduction angle $M_{j,\,type}$ is visualized in Fig. 9 together with the identified linear models. Fig. 10 exemplarily shows the results for the first and the last trial for subject S4. A clearly reduced average joint angle due to muscle fatigue can be observed in the last trial using DS. Using DS, a rapid progression of muscle fatigue is observed. In case of RC, the effects of muscle fatigue have been well compensated. This is possible until the maximally tolerable stimulation intensity is reached.

Regarding the joint angle hysteresis, only slight improvements were observed but not statistically significant ($Z = -1.753$; $p = 0.08$) in four of five subjects. We assume hysteresis effects observed are caused mainly by nonlinear elastic joint moment effects and reflexes and to a slight extend the FES-induced muscle activation itself. Only the latter can be compensated by the RC.

Though, the effects of recruitment control to the static behavior have been intensively studied, the dynamic behavior e.g. the reference-tracking performance has not been statistically evaluated. However, for all tested persons, time-series plots show a precise tracking of the desired recruitment with low delay (typically rise times of 3 to 8 sampling instants have been observed), which is well sufficient to the developed weight compensation controller.

Hence, the increased effort introduced by the additionally required EMG measurements (both in donning more electrodes and in using additional devices) is appropriate for the benefits achieved by the recruitment control. Furthermore, the availability of EMG measurements allows to estimate the voluntary contribution online, which can be provided as a feedback to the patient to improve his/her performance or used for monitoring the efficacy of a therapy. The setup might be simplified when an EMG-measurement via the stimulation electrodes becomes feasible. A first solution for the assessment of volitional muscle activity is described elsewhere [16].

3.2. FES supported shoulder abduction results

3.2.1. Healthy

The weight compensation controller has been applied to each healthy subject. Detailed time-series results of all trials of S4 are shown in Fig. 11. Hereby, for increasing trial indices, the support factor has been increased from $p_1^{WC} = 0.0$ to $p_7^{WC} = 0.6$. The last trial $j = 7$ leads to some slight overcompensation of the arm weight at lower angles, so that no further trial has been performed. The results of all trials overcompensation for all five subjects are summarized in Fig. 12. In average, a maximal support level of $p^{WC} = 0.7$ could be achieved leading to a minimal volitional effort of 22% (reduction by 78%).

3.2.2. Stroke patient

The weight compensation controller has been applied to the stroke patient. The achieved arm abduction is illustrated in Fig. 13. Without support, the patient could only achieve **6°** shoulder abduction. With arm weight support more extensive movements were possible. However, for a support factor of $p^{WC} = 1$ overcompensation of the arm weight occurred at $\vartheta = 25°$. The arm could only lowered by decreasing p^{WC}. With a reduced support of $p^{WC} = 0.75$ he could lift, hold and lower the arm voluntary up to 16°.

Please cite this article as: C. Klauer et al., A patient-controlled functional electrical stimulation system for arm weight relief, Medical Engineering and Physics (2016), http://dx.doi.org/10.1016/j.medengphy.2016.06.006

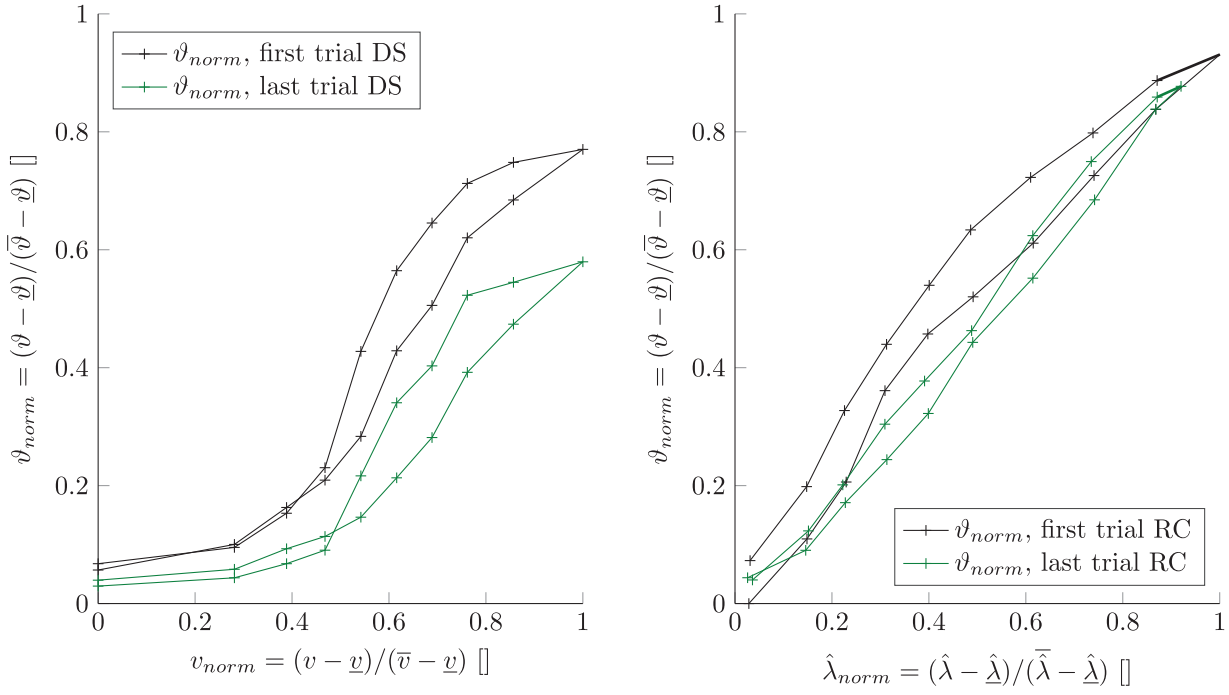

Fig. 10. Exemplary results of the first and the last trial of the fatigue comparison test for subject S4.

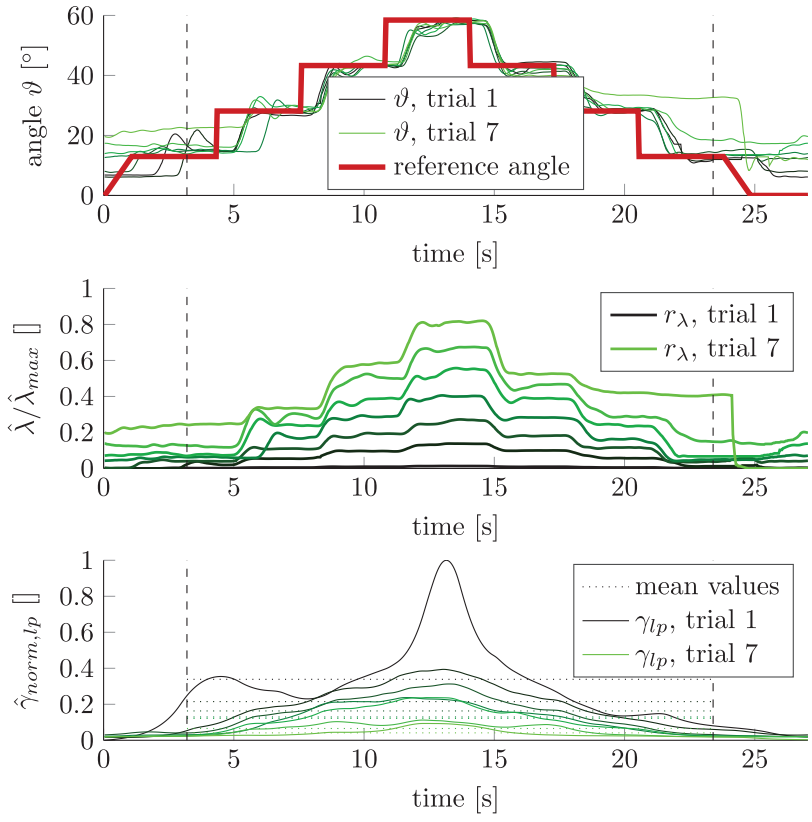

Fig. 11. Time series of measured signals during the tracking test with activated weight compensating controller in case of subject S4. The signals are aligned to the beginning of each trial. As the trial index increases, the support factor p^{WC} is increased leading to decreasing mean values of the volitional EMG activity $\hat{\gamma}$, while support is taken over by FES, indicated by the increasing recruitment level.

Please cite this article as: C. Klauer et al., A patient-controlled functional electrical stimulation system for arm weight relief, Medical Engineering and Physics (2016), http://dx.doi.org/10.1016/j.medengphy.2016.06.006

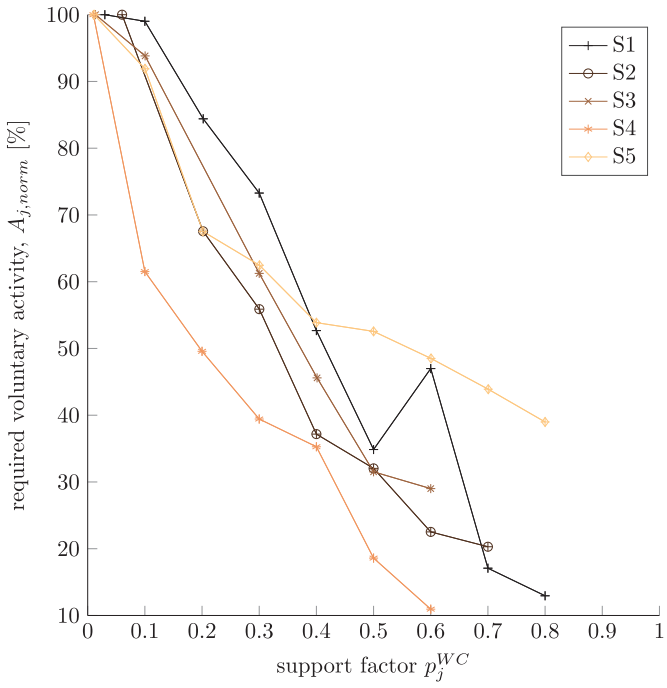

Fig. 12. Required voluntary activity for all subjects and all tested support factors p^{WC}.

4. Conclusions

To improve FES-induced muscle activation w.r.t to muscle fatigue and to the degree of linearity, we proposed feedback control of the muscular recruitment state estimated by EMG measurements. To maximize degree of linearity, we proposed an optimization procedure that adjusts two filter parameters in the estimation of the recruitment level. In experimental tests with five healthy subjects, we could show a significant improvement of linearity when comparing the stimulation intensity – angle and recruitment level – angle relationship. We could further show the compensation of the effects of muscle fatigue: In a comparative test, after 6 minutes of active FES, the average joint angle dropped by 44% ± 14 in case of non-controlled FES compared to 0% ± 12 in case of recruitment controlled FES in average for all subjects. Although healthy subjects were asked to remain passive when stimulation was on, similar tests should be repeated on a significant sample of stroke patients to verify if the same results are achieved also on subjects with a compromised sensory-motor pathway. However, the feasibility test performed on one stroke patient showed encouraging results on the applicability of the proposed controller. Future research will focus on recruitment control in multi-channel stimulation systems and the application to other muscle/ joint combinations.

To support weak residual voluntary activity in the paretic arm abduction by FES-induced muscle activation, we proposed a proportional feedback of the joint angle to control the desired recruitment level of the deltoid muscle. The system can be parameterized by a support factor that allows the system to take over muscle activation to a certain degree. Still, the user has full control of the movement as the residual activity is amplified by the control loop. An almost completely paralyzed stroke patient was able to perform arm abduction movements to an bigger extend than before. Since the maximal possible support factor is limited by hysteresis effects in the joint angle, the maximal possible support has been identified experimentally for a group of healthy subjects. A systematic approach not requiring an user-observation by the operator would be beneficial.

Future research will consider the applicability to daily live environments and complex rehabilitation exercises. A main limitation of the current solution is that the elbow was always fully extended. In a next version we will update the calculation of the desired recruitment by taking the shoulder abduction and the elbow angle as well as a simple bio-mechanical arm model into account.

In the short-term, we plan further tests on stroke patients with different degrees of paralysis. Based on our observations resulting from the application of the controller to the patient with almost completely paralyzed arm abduction, we can state that a precise measurement of the arm abduction not influenced by factors like upper body orientation is needed. This can be solved by attaching an additional IMU to the upper body.

To systematically adapt the support factor, we think of a top-level adaptive control system performing a long-term comparison

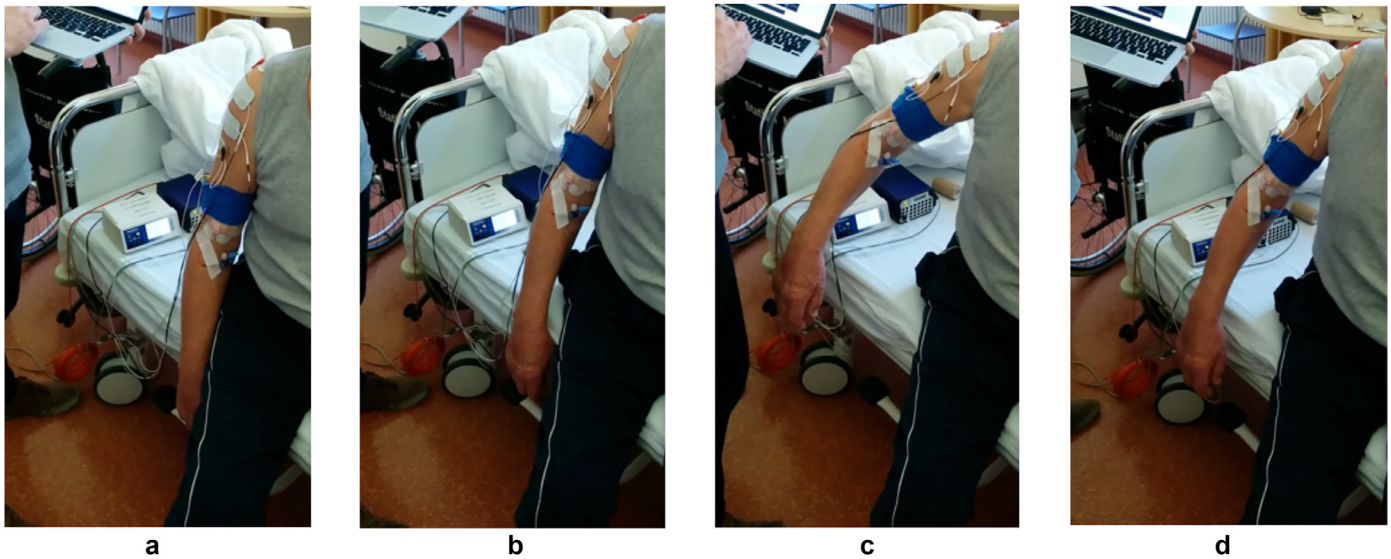

Fig. 13. Evaluation of the arm weight compensation with a stroke patient: A – rest position, B – maximal volitional shoulder abduction without support ($p^{WC} = 0$, C – voluntary initiated shoulder abduction with maximal support factor $p^{WC} = 1$ yielding overcompensation of the arm weight (return to rest position by decreasing p^{WC}), D – voluntary initiated and released arm lift with a support factor of $p^{WC} = 0.7$.

Please cite this article as: C. Klauer et al., A patient-controlled functional electrical stimulation system for arm weight relief, Medical Engineering and Physics (2016), http://dx.doi.org/10.1016/j.medengphy.2016.06.006

between the estimated voluntary EMG and the resulting joint-angle movement to automatically prevent overcompensation by adjusting the support factor to the maximal support possible.

Conflict of interest

No conflict of interest.

Ethical approval

Ethics Approval was given by the ethics committee of the Berlin Chamber of Physicians (Ärztekammer Berlin). Eth-25/15.

References

[1] Vafadar A, Côté J, Archambault P. Effectiveness of functional electrical stimulation in improving clinical outcomes in the upper arm following stroke: a systematic review and meta-analysis. Biomed Res Int 2015;2015:729768. doi:10.1155/2015/729768.
[2] Ridding M, Brouwer B, Miles T, Pitcher J, Thompson P. Changes in muscle responses to stimulation of the motor cortex induced by peripheral nerve stimulation in human subjects. Exp Brain Res 2000;131(1). 135–43
[3] Barsi G, Popovic D, Tarkka I, Sinkjaer T, Grey M. Cortical excitability changes following grasping exercise augmented with electrical stimulation. Exp Brain Res 2008;191(1):57–66. doi:10.1007/s00221-008-1495-5.
[4] Gandolla M, Ferrante S, Molteni F, Guanziroli E, Frattini T, Martegani A, et al. Re-thinking the role of motor cortex: context-sensitive motor outputs? Neuroimage 2014;91:366–74. doi:10.1016/j.neuroimage.2014.01.011.
[5] Shindo K, Fujiwara T, Hara J, Oba H, Hotta F, Tsuji T, et al. Effectiveness of hybrid assistive neuromuscular dynamic stimulation therapy in patients with subacute stroke: a randomized controlled pilot trial. Neurorehabil Neural Repair 2011;25(9):830–7. doi:10.1177/1545968311408917.
[6] Cauraugh J, Light K, Kim S, Thigpen M, Behrman A. Chronic motor dysfunction after stroke: recovering wrist and finger extension by electromyography-triggered neuromuscular stimulation. Stroke 2000;31(6). 1360–4
[7] Saxena S, Nikolić S, Popović D. An emg-controlled grasping system for tetraplegics. J Rehabil Res Dev 1995;32(1):17–24.
[8] Fujiwara T, Kasashima Y, Honaga K, Muraoka Y, Tsuji T, Osu R, et al. Motor improvement and corticospinal modulation induced by hybrid assistive neuromuscular dynamic stimulation (hands) therapy in patients with chronic stroke. Neurorehabil Neural Repair 2009;23(2). doi:10.1177/1545968308321777. 125–32
[9] Thorsen R, Spadone R, Ferrarin M. A pilot study of myoelectrically controlled fes of upper extremity. IEEE Trans Neural Syst Rehabil Eng 2001;9(2). 161–8
[10] Ambrosini E, Ferrante S, Schauer T, Klauer C, Gaffuri M, Ferrigno G, et al. A myocontrolled neuroprosthesis integrated with a passive exoskeleton to support upper limb activities. J Electromyogr Kinesiol 2014;24(2):307–17. doi:10.1016/j.jelekin.2014.01.006.
[11] Riener R, Fuhr T. Patient-driven control of fes-supported standing up: a simulation study. IEEE Trans Rehabil Eng 1998;6(2). 113–24
[12] Freeman C, Rogers E, Burridge JH, Hughes A-M, Meadmore KL. Iterative Learning Control for Electrical Stimulation and Stroke Rehabilitation. Springer; 2015.
[13] Klauer C, Raisch J, Schauer T. Linearisation of electrically stimulated muscles by feedback control of the muscular recruitment measured by evoked EMG. In: Proceedings of the 17th International Conference on Methods and Models in Automation and Robotics, IEEE. Miedzyzdroje, Poland; 2012. p. 108–13. doi:10.1109/MMAR.2012.6347902.
[14] Ambrosini E, Schauer T, Klauer C, Pedrocchi A, Ferrigno G, Ferrante S. Control system for neuro-prostheses integrating induced and volitional effort. IFAC-PapersOnLine 2015;48(20):327–32. doi:10.1016/j.ifacol.2015.10.160.
[15] Åström KJ, Wittenmark B. Computer-Controlled Systems: Theory and Design. Prentice Hall; 1997.
[16] Shalaby R, Schauer T, Liedecke W, Raisch J. Amplifier design for EMG recording from stimulation electrodes during functional electrical stimulation leg cycling ergometry. Biomed Tech (Berl) 2011;56(1):23–33. doi:10.1515/BMT.2010.055.

Please cite this article as: C. Klauer et al., A patient-controlled functional electrical stimulation system for arm weight relief, Medical Engineering and Physics (2016), http://dx.doi.org/10.1016/j.medengphy.2016.06.006